2021 27th International Conference on Mechatronics and Machine Vision in Practice (M2VIP) | 978-1-6654-3153-8/21/$31.00 ©2021 IEEE | DOI: 10.1109/M2VIP49856.2021.9665150

# Optimization For 3D Reconstruction Of Coronary Artery Tree By Two-stage Levenberg-Marquardt Algorithm

Zeyu Fu[1] Zhuang Fu[13] Zening Gong[1] Xin Feng[1] Haoran Gu[1] Rongli Xie[2] Jun Zhang[2] and Jian Fei[2]

***Abstract*— Three dimensional(3D) information acquisition and optimization of coronary artery tree is a key technology for the evaluation and diagnosis of cardiovascular disease. Based on the X-ray coronary angiography images in two directions, 3D reconstruction method establishes a projection model using the theory of perspective projection. In this study, on the basis of two-stage Levenberg-Marquardt(LM) algorithm, a novel method is employed for refinement of the 3D structure of vessel skeletons, considering deviation of angiography angle and distance. The first stage LM algorithm(LM1) optimizes the epipolar line matching error and the second stage LM algorithm(LM2) optimizes the back projection error. The experimental results show that this algorithm manages to obtain reconstruction model more accurately within a shorter time, verifying the efficacy of the proposed method.**

***Index Terms*— Optimization, 3D reconstruction, Coronary artery tree, LM algorithm**

## I. INTRODUCTION

X-ray coronary angiography is one of the most commonly utilized method to evaluate coronary stenosis and its severity, which is known as the gold standard for the diagnosis of coronary artery disease(CAD)[1]. The biggest disadvantage of X-ray imaging is that the three-dimensional structure of blood vessels is overlapped on the two-dimensional image, interferring the doctor's observation[2]. 3D reconstruction of coronary artery tree can provide more abundant medical information, which is beneficial to the quantitative description and diagnosis of disease conditions, and can guide the interventional treatment of coronary heart disease. According to the type of angiographic instrument used, 3D reconstruction of coronary artery can be classified into three classes: monoplane system, biplane system, or rotational system. Among them, the monoplane system has developed most maturely in the past dozen years[3].

Monoplane coronary angiography oprates on a C-arm system. A sequence of coronary angiography images is obtained from one angle at a time. The geometric transformation matrix between two uncalibrated monoplane angiographic images is the key of 3D reconstruction[4]. Meanwhile, the inconsistency of image acquisition time and the error of system position calibration bring great difficulties to 3D reconstruction and motion analysis. In order to refine the 3D structure of vessel skeletons, it is necessary to improve the accuracy of geometric transformation matrix.

The calibration method of angiography system proposed by G .Kristiansen is complicated, time-consuming and difficult to be popularized in clinical application[5]. Klein JL. found in his study that the error of angiography system parameters and the error of two-dimensional image processing reduced the accuracy of three-dimensional reconstruction of coronary tree[6]. S. James Chen uses branch point coordinates to optimize geometric transformation matrix to determin optimal views, nevertheless his method has limited effectiveness[7]. J.Yang proposed a nonlinear optimization method to ruduce back projection error, which took the table movement and projection geometry deviation into consideration[3]. But he takes too many parameters in his one-stage LM algorithm, which leads to coupling in calculation, slow convergence speed, and easy to fall into local optimum, resulting in vascular distortion. C.Oueslati introduce artificial interest nodes to respect the topology variation between 3D vascular trees, but this opration is difficult to implement and cannot applicate widely[8].

In order to obtain the geometric transformation matrix more accurately for uncalibrated monoplane angiographic images, this paper adopts a new nonlinear least square method based on two-stage LM algorithm. There are two main contributions of this study. First, the mathematical model of monoplane angiography is established and the matching of conjugate point pairs of epipolar lines are analyzed. Second, a novel two-stage LM algorithm is proposed and verified for the optimization of 3D reconstruction. The first stage LM algorithm(LM1) optimizes the mean epipolar line matching error and the second stage LM algorithm(LM2) optimizes the mean back projection error.

The angiogram images used in our experiment were obtained from routine medical practice. The initial parameters were read from the devices. The image preprocessing is completed before 3D reconstruction, including vessel segmentation, skeleton extraction and feature point recognition[9][10].

The rest of this paper is organized as follows. In Section II, the methodology of the proposed work will be discussed, followed by Section III, which illustrates the design and the results of the experiment. Section IV will present the conclusion.

## II. METHODS

### A. Mathematical model of monoplane angiography

*1) Perspective projection model:* Since the size of the X-ray source is much smaller than the distance between the

[1]Z. Y. Fu, Z. Fu, Z. N. Gong, X. Feng and H. R. Gu are with State Key Lab of Mechanical System and Vibration, Shanghai Jiao Tong University, Shanghai 200240, China (e-mail: {summer0528, zhfu, gongzening, fengxincn, guhaoran}@sjtu.edu.cn).

[2]R. L. Xie, J. Zhang and J. Fei are with Ruijin Hospital affiliated to Shanghai Jiao Tong University, Shanghai 200025, China (e-mail: rongli.xie@hotmail.com, 13816000547@163.com, feijian@hotmail.com).

[3]Corresponding author: Zhuang Fu.

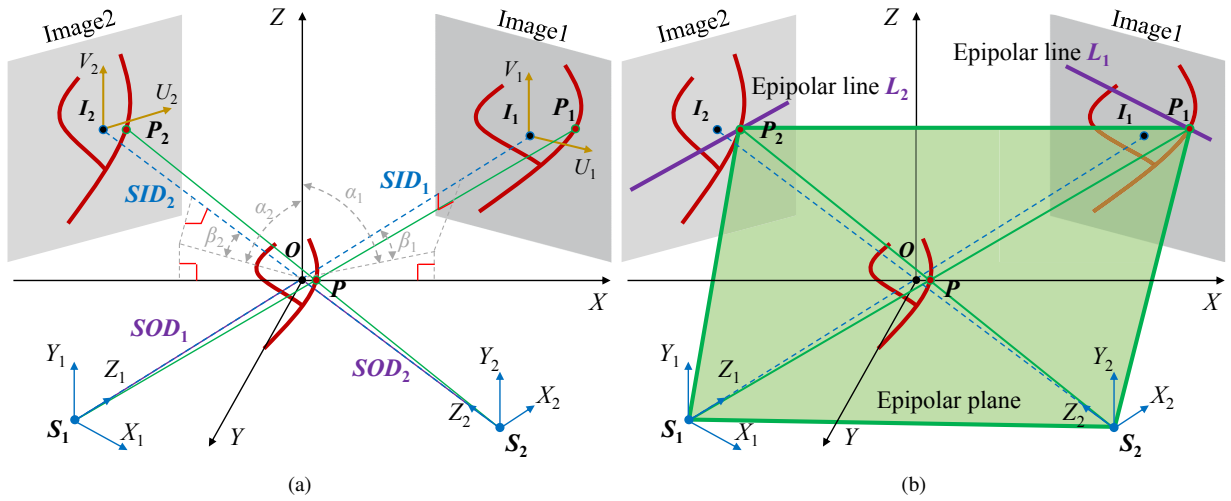


Fig. 1. Simplified model of monoplane X-ray angiography. (a) Schematic view of the angiography system from two different directions, including major parameters. (b) Schematic diagram of epipolar constraint.

X-ray source and the receiver, and for the convenience of research, the X-ray source is assumed to be an ideal point source. It emits a tapered beam of rays, and the projection axis of the rays is perpendicular to the image plane, so the X-ray radiography can be viewed as a simple one-point perspective, with the X-ray source being the extinction point. According to the principle of perspective projection[11][12], the projection model of the X-ray angiography system was established, as shown in Fig.1(a). Points $S_1$ and $S_2$ represent the positions of X-ray sources. $XYZO$ is the world coordinate system, $X_1Y_1Z_1S_1$ and $X_2Y_2Z_2S_2$ are the local coordinate systems with points $S_1$ and $S_2$ as the origin. The X-ray projection axis $S_1Z_1$ incident image1 vertically at the point $I_1$, $S_2Z_2$ incident image2 vertically at the point $I_2$. $U_1I_1V_1$ and $U_2I_2V_2$ are image coordinates. Angiography angles were recorded as $(\alpha_1, \beta_1)$ and $(\alpha_2, \beta_2)$. $\alpha_i (i = 1, 2)$ represents the LAO/RAO(Left anterior obique/Right anterior obique) angle, when $\alpha_i < 0$ it represents LAO, whereas it represents RAO. $\beta_i (i = 1, 2)$ represents the CRAN/CUAD(Cranial/Caudal) angle, when $\beta_i > 0$ it represents CRAN, whereas it represents CUAD. SID(source to image intensifier distance) and SOD(source to object distance) determine the spatial relation among sources, objects and images.

*2) Least square solution:* Assume that the projection point of space point $\boldsymbol{P}(x, y, z)$ in coordinate $X_iY_iZ_iS_i$ is $\boldsymbol{P}_i(x_i, y_i, z_i)$, in image coordinate $U_iI_iV_i$ is $\boldsymbol{p}_i(u_i, v_i)$, the translation vector between the coordinate systems is $\boldsymbol{T}_i = (0\ 0\ SOD_i)^T,\ i = 1, 2$.

Define the following matrix

$$\boldsymbol{R}_x(\theta) = \begin{pmatrix} 1 & 0 & 0 \\ 0 & cos\theta & sin\theta \\ 0 & -sin\theta & cos\theta \end{pmatrix} \tag{1}$$

$$\boldsymbol{R}_y(\theta) = \begin{pmatrix} cos\theta & 0 & -sin\theta \\ 0 & 1 & 0 \\ sin\theta & 0 & cos\theta \end{pmatrix} \tag{2}$$

According to the transformation between coordinate systems, we can get

$$\boldsymbol{P} = {\boldsymbol{R}_y}^{-1}(\alpha_i) \cdot {\boldsymbol{R}_x}^{-1}(\beta_i) \cdot (\boldsymbol{P}_i - \boldsymbol{T}_i),\ i = 1, 2 \tag{3}$$

The relation between $\boldsymbol{P}_1$ and $\boldsymbol{P}_2$ can be obtained according to equation(3)

$$\boldsymbol{P}_2 = \boldsymbol{R} \cdot (\boldsymbol{P}_1 - \boldsymbol{T}) \tag{4}$$

in which $\boldsymbol{R} = \boldsymbol{R}_x(\beta_2) \cdot \boldsymbol{R}_y(\alpha_2) \cdot \boldsymbol{R}_y^{-1}(\alpha_1) \cdot \boldsymbol{R}_x^{-1}(\beta_1)$, $\boldsymbol{T} = -\boldsymbol{R}^{-1} \cdot \boldsymbol{T}_2 + \boldsymbol{T}_1$. Let

$$\boldsymbol{R} = \begin{pmatrix} r_{11} & r_{12} & r_{13} \\ r_{21} & r_{22} & r_{23} \\ r_{31} & r_{32} & r_{33} \end{pmatrix}, \boldsymbol{T} = \begin{pmatrix} t_1 \\ t_2 \\ t_3 \end{pmatrix} \tag{5}$$

Define $\xi_i = u_i/SID_i$, $\eta_i = v_i/SID_i$, $i = 1, 2$. According to the perspective projection principle, the relation between $X_iY_iZ_iS_i$ and $U_iI_iV_i$ can be defined as

$$\begin{pmatrix} x_i \\ y_i \\ z_i \end{pmatrix} = z_i \begin{pmatrix} u_i/SID_i \\ v_i/SID_i \\ 1 \end{pmatrix} = z_i \begin{pmatrix} \xi_i \\ \eta_i \\ 1 \end{pmatrix}, i = 1, 2 \tag{6}$$

Simultaneously solve equation(4) and equation(6), The coordinates of $P_1$ satisfy the following equations

$$\begin{pmatrix} 1 & 0 & -\xi_1 \\ 0 & 1 & -\eta_1 \\ m_1 & m_2 & m_3 \\ n_1 & n_2 & n_3 \end{pmatrix} \begin{pmatrix} x_1 \\ y_1 \\ z_1 \end{pmatrix} = \begin{pmatrix} 0 \\ 0 \\ m_1t_1 + m_2t_2 + m_3t_3 \\ n_1t_1 + n_2t_2 + n_3t_3 \end{pmatrix} \tag{7}$$

in which

$$\begin{pmatrix} m_1 \\ m_2 \\ m_3 \end{pmatrix} = \begin{pmatrix} r_{11} - r_{31}\xi_2 \\ r_{12} - r_{32}\xi_2 \\ r_{13} - r_{31}\xi_2 \end{pmatrix}, \begin{pmatrix} n_1 \\ n_2 \\ n_3 \end{pmatrix} = \begin{pmatrix} r_{21} - r_{31}\xi_2 \\ r_{22} - r_{32}\xi_2 \\ r_{23} - r_{31}\xi_2 \end{pmatrix}$$

For this overdetermined equation, the least square solution can be used to obtain the optimal coordinate position of the space points. That is, for the overdetermined equation $\boldsymbol{A} \cdot \boldsymbol{P}_1 = \boldsymbol{b}$, solve $\boldsymbol{P}_1$ to minimize $\|\boldsymbol{A} \cdot \boldsymbol{P}_1 - \boldsymbol{b}\|$. Thus the least squares solution can be calculated by equation(9)

$$\boldsymbol{P}_1 = \left(\boldsymbol{A}^{\boldsymbol{T}} \cdot \boldsymbol{A}\right)^{-1} \cdot \boldsymbol{A}^{\boldsymbol{T}} \cdot \boldsymbol{b} \tag{8}$$

Finally, the coordinates of the points in the world coordinate system can be obtained through equation(3) to realize the 3D reconstruction.

*3) epipolar constraint:* There is a certain constraint relation between two images of the same scene obtained from two different perspectives, which is usually called the epipolar geometric relation. Fig.1(b) shows the constraint diagram of the epipolar lines. The space point $\boldsymbol{P}$, X-ray source $\boldsymbol{S}_1$ and $\boldsymbol{S}_2$ form a plane, which is called the epipolar plane. The epipolar plane intersects with image1 and image2 to get two epipolar lines $\boldsymbol{L}_1$ and $\boldsymbol{L}_2$. $\boldsymbol{P}_1$ and $\boldsymbol{P}_2$ are conjugate point pairs.

According to the principle of perspective projection imaging and epipolar constraint[13], the conjugate point $\boldsymbol{P}_2$ on image2 must be located on the epipolar line $\boldsymbol{L}_2$ corresponding to point $\boldsymbol{P}_1$. In coronary angiography, branch points, cross points and endpoints in blood vessels are most commonly selected as conjugate point pairs, as shown in Fig.4(a)(b).

Deviations of angiography angle and distance bring epipolar line matching error. Through the equation of epipolar lines, this error can be calculated.

Combining equation(4) and equation(6), we can get

$$\begin{pmatrix} x_2 \\ y_2 \\ z_2 \end{pmatrix} = z_2 \begin{pmatrix} \xi_2 \\ \eta_2 \\ 1 \end{pmatrix} = \begin{pmatrix} z_1 a_1 - b_1 \\ z_1 a_2 - b_2 \\ z_1 a_3 - b_3 \end{pmatrix} \tag{9}$$

in equation(9), $a_i = r_{i1}\xi_1 + r_{i2}\eta_1 + r_{i3}$, $b_i = r_{i1}t_1 + r_{i2}t_2 + r_{i3}t_3$, $i = 1, 2, 3$. Solve this equation and the epipolar line function of $\boldsymbol{L}_2$ can be shown as below

$$\xi_2(a_3b_2 - a_2b_3) + \eta_2(a_1b_3 - a_3b_1) + (a_2b_1 - a_1b_2) = 0 \tag{10}$$

Define the distance between $\boldsymbol{p}_2(u2, v2)$ and $\boldsymbol{L}_2$ as the epipolar line matching error. It can be calculated by

$$d_2 = \frac{|\xi_2(a_3b_2 - a_2b_3) + \eta_2(a_1b_3 - a_3b_1) + (a_2b_1 - a_1b_2)|}{\sqrt{(a_3b_2 - a_2b_3)^2 + (a_1b_3 - a_3b_1)^2}} \tag{11}$$

Reducing the value of $d_2$ will also reduce the error of 3D reconstruction.

## B. Back projection

As shown in Fig.2, according to the conjugate points $\boldsymbol{p}_1$ and $\boldsymbol{p}_2$ in the two-dimensional image plane, the three-dimensional point $\boldsymbol{P}'$ are reconstructed and projected onto image1 and image2 respectively to obtain the projection point pairs $\boldsymbol{p}'_1$ and $\boldsymbol{p}'_2$. If the reconstruction is accurate, point $\boldsymbol{p}_1$ in image1 should be close to $\boldsymbol{p}'_1$, and point $\boldsymbol{p}_2$ in image2 should be close to $\boldsymbol{p}'_2$. Therefore, the back projection error of 3D reconstruction can be evaluated by the length of line segment $p_1p'_1$ and $p_2p'_2$ on the two-dimensional image plane, denote as

$$\varepsilon(\boldsymbol{P}, \boldsymbol{P}') = \|\overrightarrow{p'_1p_1}\| + \|\overrightarrow{p'_2p_2}\| \tag{12}$$

in which $\|\overrightarrow{p'_1p_1}\|$ represents the Euclidean distance between $\boldsymbol{p}_1$ and $\boldsymbol{p}'_1$. Reducing the value of $\varepsilon$ will also reduce the error of 3D reconstruction.

The mean back projection error is the most commony used criterion to evaluate the accuracy of coronary artery 3D reconstruction[6].

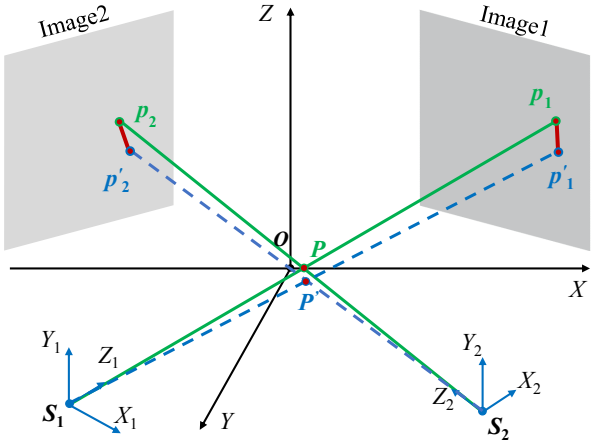


Fig. 2. Back projection model. $\boldsymbol{P}$ is the actual point and $\boldsymbol{P}'$ is the reconstruction point, $p_1p'_1$ and $p_2p'_2$ are back projection errors.

## C. Two-stage LM algorithm

According to equation(3) and equation(6), the parameters need to be optimized are $\alpha_i$, $\beta_i$, $SOD_i$ and $SID_i$, $i = 1, 2$. Let $\boldsymbol{VAR} = [\alpha_i, \beta_i, SOD_i, SID_i]$. On the basis of equation(11), the optimization function of epipolar line matching error can be formulated as

$$argminF_1(\boldsymbol{VAR}) = \sum_{j=1}^{M} d_{2j}^2 \tag{13}$$

Similarly, on the basis of equation(12), the optimization function of back projection error can be formulated as

$$argminF_2(\boldsymbol{VAR}) = \sum_{k=1}^{N} \|\overrightarrow{p'_{1k}p_{1k}}\|^2 + \|\overrightarrow{p'_{2k}p_{2k}}\|^2 \tag{14}$$

where $M$ and $N$ are the numbers of calculated points.

Obviously, objective function $F_1$ and $F_2$ belong to the nonlinear least squares problem, many different nonlinear search algorithms can be used to solve such problems. Commonly used methods mainly include the fastest descent method, conjugate gradient descent method, Gause-Newton algorithm and Levenberg-Marquardt(LM) algorithm, etc[14][15]. Among them, LM algorithm is also known as the damped least square method. Compared with other methods, L-M method has faster convergence speed and is more robust, so it is more commonly used.

In this paper, the traditional LM algorithm is simplified. For normalized function $F(x) = \sum_{i=1}^{m} f_i(x)^2$, the main process of our algorithm is shown in Algorithm1. Where **H** is the Hessian matrix and **J** is the Jacobian matrix. Input variables include initial parameter $x_0(\boldsymbol{VAR}_0)$, damper factor $\lambda$, constant factor $\beta$, maximum permissible error(MPE) $\varepsilon$ and maximum iterations $N$.

Due to the complexity of the process of back projection and LM algorithm, if the back projection error is directly calculated, once the initial parameter accuracy is low, setting a high convergence precision will consume much time and more badly the result could fall into local optimum, resulting in vascular distortion.

**Algorithm 1** Simplified LM algorithm

**Input:** $x_0$, $\lambda$, $\beta$, $\varepsilon$, $N$
**Output:** $x_{min}$, $F_{min}$

$x_{curr} := x_0$, $F_{curr} := F(x_0)$
**for** $iter := 1 \rightarrow N$ **do**
  $\Delta x := -[\mathbf{H}(x_{curr}) + \lambda \mathbf{I}]^{-1} \mathbf{J}^T(x_{curr}) f(x_{curr})$
  $x_{new} := x_{curr} + \Delta x$, $F_{new} := F(x_{new})$
  **if** $F_{new} < F_{curr}$ **then**
    $x_{curr} := x_{new}$
    **if** $\|\Delta x\| < \varepsilon$ **then**
      $x_{min} := x_{curr}$, $F_{min} := F_{new}$
      **break**
    $F_{curr} := F_{new}$, $\lambda := \lambda / \beta$
  **else**
    **if** $\|\Delta x\| < \varepsilon$ **then**
      $x_{min} := x_{curr}$, $F_{min} := F_{new}$
      **break**
    $\lambda := \lambda * \beta$
**return** $x_{min}$, $F_{min}$

Therefore, in this study, we propose a two-stage LM algorithm. In the first stage(LM1), we set a relatively low convergence precision to optimize $F_1$, this process converges quickly and gets temporary parameters. In the second stage(LM2), based on the result in LM1, we set a relatively high convergence precision to optimize $F_2$, this process converges slowly and gets final optimized parameters. The whole procedure is shown in Fig.3.

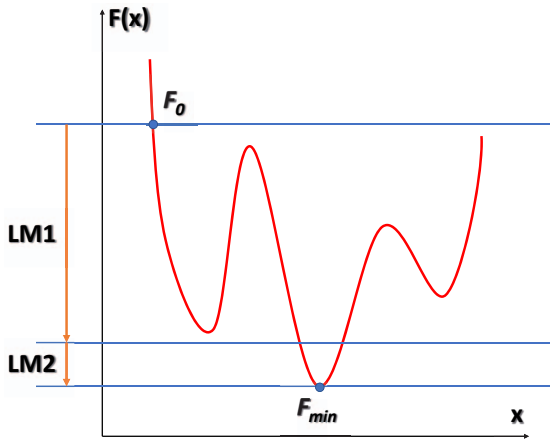


Fig. 3. Two-stage LM algorithm and its convergence procedure

## III. EXPERIMENT

In order to verify the reliability of the proposed method, the experiment is divided into three parts. Firstly, the angiography images were processed and the conjugate point pairs were selected. Secondly, the mean epipolar line matching error is optimized. At last, the mean back projection error is optimized. And the reconstruction model is established.

The experiment was programmed in Matlab R2020a, ran on a low cost PC with a 3.60GHz Intel(R) Core(TM) i5-8600K CPU and 16G Memory.

### A. Conjugate point pairs selecting

Before 3D reconstruction, it is necessary to process the initial angiography images, including vessel segmentation, skeleton extraction and feature point recognition. Fig.4(a)(b) are angiography images token from LAO/CRAN view and RAO/CRAN view of the same scene, the feature points are marked on them, and the extracted skeletons are shown on Fig.4(c)(d). According to the research by F.Cherieta, the number of feature points selected in the optimization process is not the more the better[16], so we took 6 branch points as conjugate point pairs.

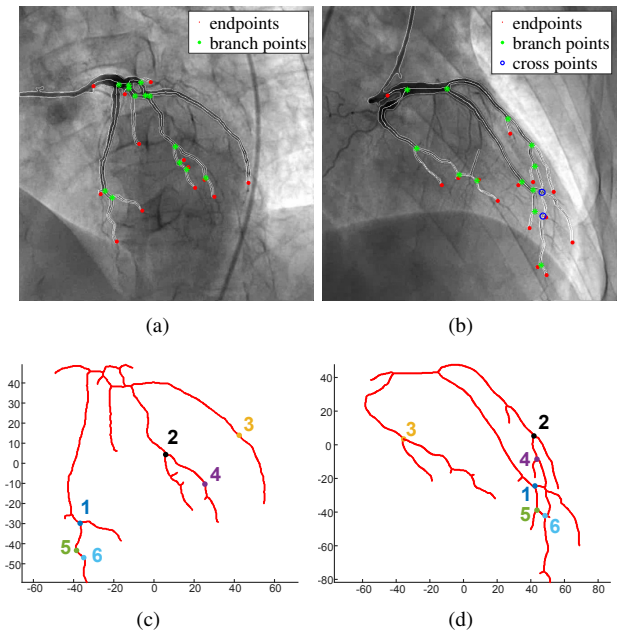


Fig. 4. Feature point recognition and conjugate point pairs selecting. (a), (b) are extracted skeletons and feature points in LAO/CRAN view and RAO/CRAN view. (c), (d) are skeletons transformed into image coordinate $UIV$, and selected conjugate point pairs.

The initial epipolar line matching error is shown on Fig.5(a), the back projected errors of each image are shown on Fig.5(d)(g). Due to relatively large deviations of initial parameters $\boldsymbol{VAR}_0$ in this experiment, the coincidence degree between the backprojected skeleton and the original skeleton is poor, which could cause serious distortion of the 3D reconstruction.

The rest of experiment will optimize these errors.

### B. Epipolar line matching error optimization

Compared with back projection error, epipolar line matching error is much easier to calculate and costs less time for the following reasons:

- Back projection error needs to do the complex matrix manipulation twice(forward and backward), epipolar line matching error just need once(forward).

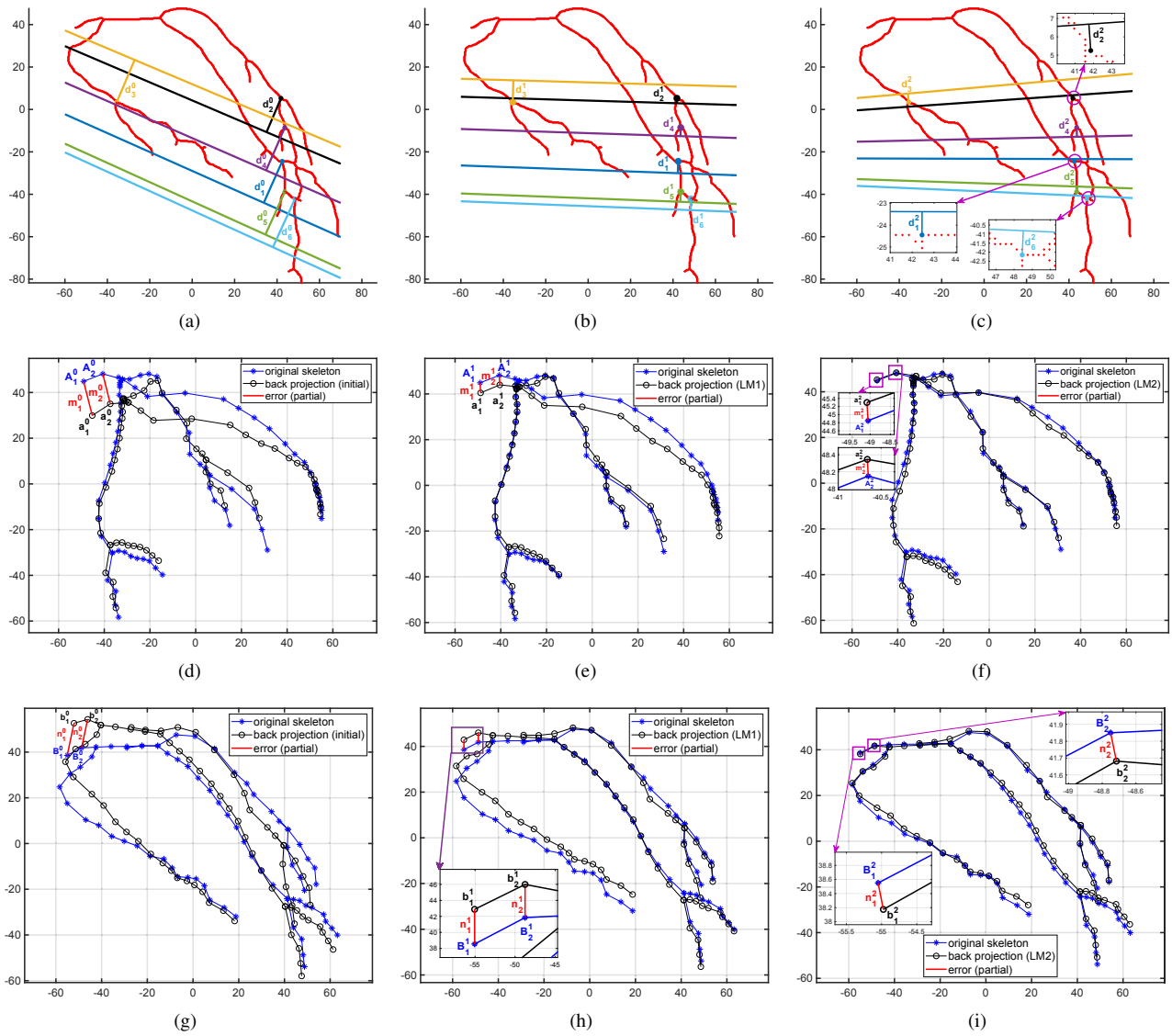


Fig. 5. Epipolar line matching errors $d_i^j$ and back projection errors $m_i^j$, $n_i^j$ in different stages. (a), (b), (c) are epipolar line matching errors before optimization, after LM1 and after LM2. (d), (e), (f) are back projection errors in LAO/CRAN view before optimization, after LM1 and after LM2. (g), (h), (i) are back projection errors in RAO/CRAN view before optimization, after LM1 and after LM2.

- Back projection error calculates multiple points to insure the authenticity, epipolar line matching error just takes several conjugate point pairs(in this paper 6) into consideration.
- In our method the epipolar line matching error optimization just meed to get temporary parameters $\boldsymbol{VAR}_1$, thus the convergence precision is relatively low comparing with back projection error optimization.

Therefore, we set relatively large $\varepsilon_1$ of Algorithm1 in LM1. This procedure consumes few time, as listed in Tab.I. After the optimization of LM1, the epipolar line matching error is shown on Fig.5(b), the back projected errors of each image are shown on Fig.5(e)(h). It can be found that the coincidence degree between the backprojected skeleton and the original skeleton increases, but in some points it still needs to be refined.

### C. Back projection error optimization

To ensure the accuracy of feature points reconstruction, in addition to selecting reference points evenly on each vessel, we repeat the selection near the feature points. Moreover, we set relatively small $\varepsilon_2$ of Algorithm1 in LM2. This procedure consumes more time than LM1, as listed in Tab.I. After the optimization of LM2, the epipolar line matching error is shown on Fig.5(c), the back projected errors of each image are shown on Fig.5(f)(i). Obviously the result is much bettrer, most of the errors can only be seen by zooming in. To make it more intuitive, we back project the 3D structure onto original iamges, as show in Fig.6.

For a more detailed analysis, the time consuming data of LM1 and LM2 are recorded in Tab.I. And the errors after each optimization are listed in Tab.II. As a comparison, we take a one-stage LM algorithm[3] experiment and also show

the result. It can be seen that in the case of a relatively large initial error, one-stage LM algorithm cannot converge to the specified precision within the maximum iteration, this also results in significant time consumption.

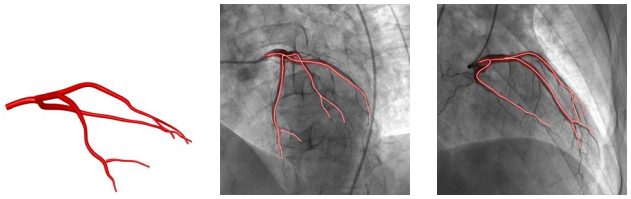

(a) (b) (c)

Fig. 6. (a) Reconstructed 3D model in world coordinate system $XYZO$, projected vertically along the $Z$ axis. (b), (c) are back projections on initial images, the red parts are vascular perspectives and the white parts are their skeletons. (b) is from LAO/CRAN view and (c) is from RAO/CRAN view.

TABLE I
TIME CONSUMING OF DIFFERENT ALGORITHMS

| algorithms | | maximum iterations | actual iterations | time cost(s) | total(s) |
|---|---|---|---|---|---|
| 2-stage LM | LM1 | 100 | 23 | 786.4 | 6476.3 |
| | LM2 | 100 | 36 | 5689.9 | |
| 1-stage LM | | 100 | 100 | 15678.3 | 15678.3 |

TABLE II
ERROR STATISTICS OF EUCLIDEAN DISTANCES BETWEEN EXTRACTED AND BACKPROJECTED[1][2]

| algorithms | maximum | minimum | Mean | RMS |
|---|---|---|---|---|
| before optimization | 15.7895 | 0.2366 | 5.2212 | 8.6965 |
| 2-stage LM | 0.8767 | 0.0004 | 0.1543 | 0.2698 |
| 1-stage LM | 2.6316 | 0.0003 | 0.3857 | 0.5141 |

[1] Errors are the sum of two images.
[2] Units of all datas are millimeters.

From Tab.I, the computational efficiency is increased by 58.7%. And from Tab.II, the reconstruction accuracy is increased by 47.5% within 100 iterations. These verifies the reliability of the method.

## IV. CONCLUSIONS

In this paper, a two-stage LM algorithm is adopted for the optimization of coronary artery tree 3D reconstruction. Specifically, the mathematical model of monoplane angiography is established and analyzed, and the formulations of epipolar line matching error and back projection error are derived. On this basis, the LM algorithm is simplified and experimented. The reconstruction result shows that the proposed method improves computational efficiency and reconstruction accuracy, it is more applicable for uncalibrated monoplane angiographic images.

## ACKNOWLEDGMENT

This work was greatly supported by the National Natural Science Foundation of China(Grant No. 61973210) and the Medical-engineering Cross Projects of SJTU(Grant Nos. YG2019ZDA17, ZH2018QNB23).

## REFERENCES

[1] Çimen, Serkan, et al. "Reconstruction of coronary arteries from X-ray angiography: A review." Medical image analysis 32 (2016): 46-68.
[2] Green, Nathan E., et al. "Three-dimensional vascular angiography." Current problems in cardiology 29.3 (2004): 104-142.
[3] Yang, Jian, et al. "Novel approach for 3-D reconstruction of coronary arteries from two uncalibrated angiographic images." Ieee transactions on image processing 18.7 (2009): 1563-1572.
[4] Zhang, Tianxu, et al. "Cardiovascular Tree Recognition and its Three-Dimensional Reconstruction from Monoplane X-Ray Angiography Based on Spatio-Temporal Constraints." 2019 12th International Congress on Image and Signal Processing, BioMedical Engineering and Informatics (CISP-BMEI). IEEE, 2019.
[5] Kristiansen, G., et al. "Accuracy and precision of the analytic calibration method in quantitative coronary arteriography." Computers in Cardiology 1996. IEEE, 1996.
[6] Klein, J. Larry, et al. "A quantitative evaluation of the three dimensional reconstruction of patients' coronary arteries." The International Journal of Cardiac Imaging 14.2 (1998): 75-87.
[7] Chen, S. James, and John D. Carroll. "3-D reconstruction of coronary arterial tree to optimize angiographic visualization." IEEE transactions on medical imaging 19.4 (2000): 318-336.
[8] Oueslati, Chaima, et al. "3D reconstruction of coronary arteries from rotational X-ray angiography." (2018).
[9] Schaap, Michiel, et al. "Standardized evaluation methodology and reference database for evaluating coronary artery centerline extraction algorithms." Medical image analysis 13.5 (2009): 701-714.
[10] Sui, Chenxin, et al. "A Novel Method for Vessel Segmentation and Automatic Diagnosis of Vascular Stenosis." 2019 IEEE International Conference on Robotics and Biomimetics (ROBIO). IEEE, 2019.
[11] Blondel, Christophe, et al. "Reconstruction of coronary arteries from a single rotational X-ray projection sequence." IEEE Transactions on Medical Imaging 25.5 (2006): 653-663.
[12] Liao, Rui, et al. "3-D reconstruction of the coronary artery tree from multiple views of a rotational X-ray angiography." The international journal of cardiovascular imaging 26.7 (2010): 733-749.
[13] Dumay, Adrie CM, Johan HC Reiber, and Jan J. Gerbrands. "Determination of optimal angiographic viewing angles: basic principles and evaluation study." IEEE transactions on medical imaging 13.1 (1994): 13-24.
[14] Moré, Jorge J. "The Levenberg-Marquardt algorithm: implementation and theory." Numerical analysis. Springer, Berlin, Heidelberg, 1978. 105-116.
[15] Foresee, F. Dan, and Martin T. Hagan. "Gauss-Newton approximation to Bayesian learning." Proceedings of International Conference on Neural Networks (ICNN'97). Vol. 3. IEEE, 1997.
[16] Cheriet, F., and J. Meunier. "Self-calibration of a biplane X-ray imaging system for an optimal three dimensional reconstruction." Computerized medical imaging and graphics 23.3 (1999): 133-141.